[46]B. Y. Tong, Phys. Rev. A 1, 52 (1970).
[47]B. Y. Tong and S. Y. Tong, J. Chem. Phys. 54, 1317 (1971).
[48]T. C. Wong and B. Y. Tong, Bull. Am. Phys. Soc. 17, 595 (1972).
[49]J. Zittartz and J. S. Langer, Phys. Rev. 148, 741 (1966).
[50]J. Ziman, in *Solid State Physics*, edited by H. Ehrenreich, F. Seitz, and D. Turnbull (Academic, New York, 1971), Vol. 26, pp. 1–101.
[51]D. Weaire, Phys. Rev. Letters 26, 1541 (1971).
[52]R. E. Borland, Proc. Phys. Soc. (London) 78, 926 (1961).
[53]L. I. Schiff, *Quantum Mechanics*, 3rd ed. (McGraw-Hill, New York, 1968), p. 123.

PHYSICAL REVIEW B VOLUME 6, NUMBER 12 15 DECEMBER 1972

Acoustic Geometric and Acoustic Cyclotron Resonances in Gallium

C. Alquié and J. Lewiner
Laboratoire d'Electricité Générale, Ecole Supérieure de Physique et de Chimie, Paris, France
(Received 3 April 1972)

Acoustic geometric and acoustic cyclotron resonances in high-purity single crystals of gallium were investigated at 1.3 °K and in the normal geometry where the magnetic field is perpendicular to the wave vector of the ultrasonic waves. These waves, polarized longitudinally and of frequencies in the range 60–400 MHz, were propagated along the three principal crystallographic axes a, b, and c of gallium. The extremal dimensions of the Fermi surface in the k_ak_b, k_bk_c, and k_ck_a planes, obtained by measuring the periodicity $\Delta(1/H)$, of the geometric-resonance oscillations, are compared with the predictions of the augmented-plane-wave and pseudopotential models. The results are in good agreement with the values given by the pseudopotential model. A map of effective masses in the ab, bc, and ca planes, obtained from acoustic-cyclotron-resonance experiments, is given. These data are compared to those of Moore, who used the Azbel'-Kaner cyclotron resonance (AKCR). Some branches of effective masses were found which have not been observed by AKCR and, reciprocally, many resonances observed by AKCR were not observed in the present work.

I. INTRODUCTION AND THEORY

Although many experimental studies of the Fermi surface of gallium[1] have already been done, this surface, which appears to be a very complicated one, is still far from well known. The methods which have been used to investigate its properties include de Haas–van Alphen effect, magnetoresistance, magnetoacoustic effect, cyclotron resonance, and others. The comparison of the experimental data with the theoretical models proposed for gallium shows that, whereas the nearly free-electron model[2] is not confirmed, the augmented-plane-wave model (APW)[3] is in better agreement with available data. Recently, Reed[4] made some calculations using the pseudopotential model. The form factor was adjusted in order to give the best fit between the calculated surface and the experimental results.

First ultrasonic measurements on gallium were carried out by Roberts,[5] who was the first to observe acoustic cyclotron resonance (ACR) in single crystals of gallium. Some data were published,[6–9] too, on the shape of the Fermi surface determined by acoustic geometric resonance. ACR was also further investigated[10–12] and led to the knowledge of some effective masses of the carriers.

In the present work we have studied the properties of gallium by propagating longitudinal ultrasonic waves along the three principal crystallographic axes of high-purity single crystals. All the experiments were made in the so-called normal geometry where the magnetic field H is perpendicular to the ultrasonic wave vector $\vec{q}$. The ultrasonic frequencies used ranged from 60 to 400 MHz, which corresponds to $ql \gg 1$, and $\omega\tau \cong 1$ or $\omega\tau > 1$ (l is the mean free path of the electrons; it is related to the collision time τ by $l = \tau v_F$, where v_F is the Fermi velocity).

Before presenting the experimental data, we will review the basic results of the theory of the magnetoacoustic interaction, using the formalism developed by Cohen, Harrison, and Harrison (CHH).[13]

At low temperatures, the attenuation of an ultrasonic wave in a metal is due to mainly the electron-phonon interaction. Instead of a real metal, we consider a gas of free electrons moving through a uniform background of positive charges. The interaction between the sound wave and the electrons takes place via the electromagnetic field associated with the wave. Under such conditions it was shown in Ref. 13 that the attenuation α of a longitudinal wave, propagated perpendicularly to a

magnetic field $\vec{H}$, is proportional to the first diagonal component S_{11} of a tensor S. S_{11} can be expressed in terms of the components of an effective conductivity tensor σ' by the relation

$$S_{11}=\mathrm{Re}\left(\frac{\sigma'_{22}+i\beta}{\sigma'_{11}\sigma'_{22}+(\sigma'_{12})^2+i\beta\sigma'_{11}-1}\right) , \quad (1)$$

where $\beta=\omega c^2/4\pi\sigma_0 v_s^2$ is $2\pi^2$ times the ratio of the classical skin depth to the sound wavelength λ, σ_0 is the normal dc conductivity, and v_s is the sound velocity. It was assumed here that $\gamma=\beta(v_s/c)^2 \ll 1$ (if $\omega\simeq 10^8$ Hz and $\sigma_0\simeq 10^{12}\ \Omega^{-1}\ \mathrm{cm}^{-1}\simeq 9\times 10^{21}$ sec^{-1}, then $\gamma\simeq 10^{-15}$) and that $\gamma\ll|\sigma'_{11}|$ (which means that the screening occurs because of large conductivity).

The components of the tensor σ' can be written as sums of Bessel functions $J_n(X)$, where $X=qv_F/\omega_c=qR=(\omega/\omega_c)(v_F/v_s)$. In this expression ω_c is the cyclotron frequency and R is the radius of the orbit of an electron moving perpendicularly to the magnetic field. If m^* is the effective mass of this electron, then $\omega_c=eH/m^*c$. Depending on the value of X, two types of effects can occur, called geometric or cyclotron resonance.

A. Geometric Resonance

Geometric resonance is related to a spatial coherence between the extremal dimensions of the electronic orbits and the sound wavelength. It occurs when the radius of the classical orbit R is of the order of λ; this implies $X\simeq 1$, and $\omega_c\gg\omega$ because $v_F\gg v_s$. Moreover, ql must be larger than unity so that the electrons can travel over several orbits before being scattered. With these conditions it was shown in Ref. 13 that the maxima of S_{11} occur when $X=n\pi$. If H_n is the value of the magnetic field corresponding to the nth maximum of attenuation, it follows that $1/H_n=ne\lambda/2\hbar kc$. This can be rewritten as a relation between the extremal radius of the (nonspherical) Fermi surface in the q×H direction and the period $\Delta(1/H)$ of the oscillations of the attenuation:

$$k_{\mathrm{ext}}=\lambda e/2\hbar c\,\Delta(1/H) . \quad (2)$$

Substituting in (2) the experimentally determined value of the periodicity $\Delta(1/H)$, one can calculate k_{ext}.

B. Acoustic Cyclotron Resonance

This effect occurs when the cyclotron frequency ω_c is of the order of magnitude of the ultrasonic frequency ω, so that X is much larger than unity. The collision time must be larger than the period of rotation of the electron; this implies that $\omega\tau>1$. Under these conditions S_{11} can be rewritten in the form

$$S_{11}=\tfrac{1}{6}\pi\, ql\ \mathrm{Re}\coth\left(\frac{(1-i\omega\tau)\pi}{\omega_c\tau}\right) . \quad (3)$$

It is seen that S_{11} is now an oscillating function of ω/ω_c, with maxima occurring whenever $\omega=n\omega_c$, so that the resonance condition is

$$1/H_n=ne/m^*c\,\omega.$$

This implies that the ultrasonic attenuation in ACR experiments is once again periodic in $1/H$ and that the value of the effective mass of the carrier can be expressed in terms of the free-electron mass m_0 by the relation

$$m^*/m_0=e/[cm_0\omega\Delta(1/H)] . \quad (4)$$

II. EXPERIMENTAL TECHNIQUE

A. Experimental Setup

A standard ultrasonic-pulse-echo technique was used. The measuring frequencies used could be chosen within the range 50–400 MHz. The transducer, an X-cut quartz crystal with the fundamental resonance at 14 MHz, was bonded to the crystal with Dow Corning 510 silicone grease.

Two setups were used to create the magnetic field: For low fields, up to 300 Oe, a pair of Helmholtz coils was used. (The value of the field was defined to better than 1 Oe.) For high fields, up to 7000 Oe, an iron-core magnet was used. In both cases the direction of the magnetic field was kept in a plane perpendicular to the wave vector $\vec{q}$ and could be rotated in this plane. The measurements were made every 2 deg. In order to help the analysis of the data, two sweeps were used; one linear in H and another one linear in $1/H$.

The field dependence of the ultrasonic attenuation was studied by monitoring the amplitude of a selected echo, either on an X-Y recorder as a function of H, or on a Y-T one as a function of $1/H$. The temperature of the sample was lowered to 1.3 °K in order to increase the collision time.

B. Preparation of Samples

The samples were grown from 99.999%- and and 99.999 99%-initial-purity gallium. The molten gallium was placed in a cylindrical plexiglass mold

TABLE I. Physical characteristics of the samples.

Sample	Initial purity (%)	Axis	Thickness at 300 °K (mm)
a1	99.999 99	*a*	4.895 ± 0.005
b1	99.999 99	*b*	4.875 ± 0.005
b2	99.999 99	*b*	4.880 ± 0.005
c1	99.999	*c*	10.260 ± 0.005
c2	99.999 99	*c*	10.240 ± 0.005

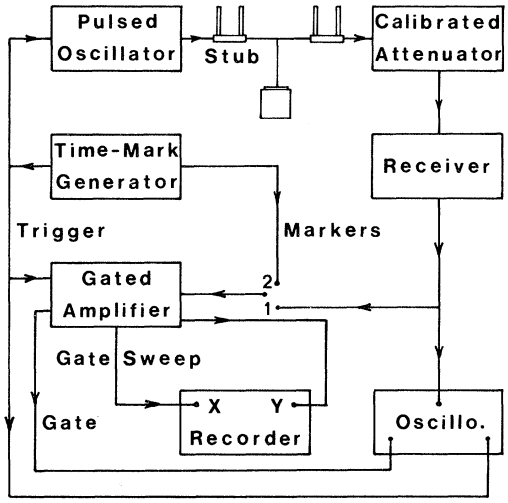

FIG. 1. Block diagram of the experimental setup used to measure the velocity of sound.

and seeded at one end with a crystal of known orientation. The axis of the cylinder was aligned to within 1 deg with one of the three principal crystallographic axes a, b, or c. The orientation of the single crystals was checked by x rays using the Laue method. In this manner we prepared 10-mm-diam cylinders of 5- or 10-mm length. The physical parameters of the different samples which were used are listed in Table I.

C. Measurement of Velocity of Sound

In order to calculate k_{ext} using Eq. (2), it is necessary to know λ, which means measuring the velocity of longitudinal waves along the a, b, and c axes. A block diagram of the experimental setup is given in Fig. 1.

A quartz-crystal-controlled time-mark generator produces a triggering pulse for the whole system. The gate position of a gated amplifier is swept during an interval of time containing as many echoes as possible. After integration the voltage seen by the gate is recorded as a function of the position of the gate. Such a recording is shown in Fig. 2(a). Markers produced by the time-mark generator are then recorded using exactly the same system [Fig. 2(b)]. This gives a time calibration for the recording. If d is the thickness of the sample and t_0 the time separating two successive echoes, v_s is given by the relation $v_s = 2d/t_0$.

The measured velocities at 295, 77, and 4.2 °K, for an ultrasonic frequency equal to 14 MHz, are given in Table II. The d values used for calculations have been corrected for thermal contraction. One should consider also the effect of bonding between the transducer and the sample which tends to increase the observed transit time of an echo. Such an effect has been discussed by Overton and Gaffney[14] and McSkimin.[15] In our case it leads to a relative correction of the order of one part per thousand. We estimate, however, that the experimental uncertainty of the velocity values is about ±0.6%.

TABLE II. Measured velocities of longitudinal ultrasonic waves along the three principal axes of gallium. Frequency: 14 MHz; units: 10^3 m/sec.

Axis \ T (°K)	295	77	4.2
a	4.04 ± 0.03	4.23 ± 0.03	4.215 ± 0.03
b	3.84 ± 0.03	3.99 ± 0.03	4.10 ± 0.03
c	4.72 ± 0.03	4.91 ± 0.03	4.91 ± 0.04

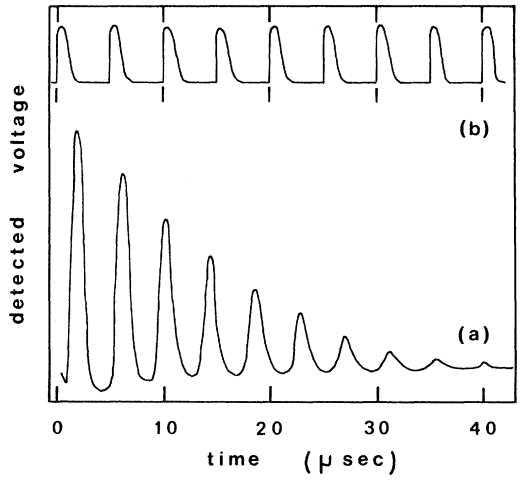

FIG. 2. Example of a recording used to measure the velocity of sound. (a) Amplitude of the successive echoes; (b) time calibration of the X coordinates. Markers at 5 μsec, f=14 MHz, T=4.2 °K; thickness of the sample (at 300 °C): 10.24 mm.

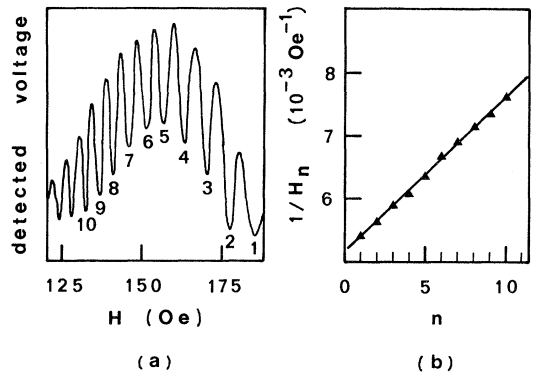

FIG. 3. (a) Geometric-resonance oscillations observed on sample b1, for $\vec{q} \parallel \vec{b}$, f=158 MHz, T=1.25 °K. (b) Corresponding curve $1/H_n = f(n)$.

Our results are in good agreement with those previously obtained at 77 °K using a transducer technique.[6,7] However, our values are systematically smaller (about 1.5%) than the results of Lyall and Cochran[16] who used a transducerless technique. The discrepancy cannot be explained by differences in measuring techniques.

III. EXPERIMENTAL RESULTS

A. General Procedure

In order to measure the periods $\Delta(1/H)$ of the ultrasonic-attenuation oscillations, a voltage proportional to the amplitude of an echo is recorded as a function of the applied magnetic field. Such a recording is shown in Fig. 3(a). Let H_n be the value of the magnetic field corresponding to the nth maximum of the attenuation (i.e., minimum of amplitude). The plot $1/H_n = f(n)$ obtained from the oscillations shown in Fig. 3(a) is drawn in Fig. 3(b). It is a straight line with a slope of $\Delta(1/H)$.

For a given orientation of the magnetic field and of the wave vector $\vec{q}$ with respect to the a, b, or c axes, several periods can be found superimposed. Two problems arise: First, one has to decide which of the oscillations are due to geometric resonance and which to ACR; second, one has to determine the oscillation periods for each case.

The problem of separating geometric oscillations from ACR can be solved by taking into account the following:

(i) ACR occurs when $\omega \simeq \omega_c$, while geometric resonance is expected when $X \simeq 1$, which means $\omega \ll \omega_c$. This implies that ACR oscillations appear at lower fields than geometric-resonance oscillations.

(ii) The theoretical line shapes are very different. However, it must be admitted that frequently two oscillations of the same type are superposed, so that the characteristic shapes do not appear very clearly.

(iii) The value of k_{ext}, calculated erroneously from ACR oscillations, is about ten times smaller than the usual values of k_{ext}.

(iv) ACR appears at $\omega\tau > 1$. This condition is more restrictive than that of $ql > 1$, required to observe geometric resonance. In our experiments, ql is larger than 100, but $\omega\tau$ is only of the order of 5 or 10. So ACR oscillations are much more sensitive to a variation of the mean free path of the electrons or of the ultrasonic frequency than geometric-resonance oscillations. The comparison of the oscillations observed at a given orientation of the sample for different purities, temperatures, or ultrasonic frequencies enables us to identify their origin without ambiguity.

In the course of separation of the different oscillations either in geometric or in cyclotron resonance, many situations can be encountered.

(a) The oscillations appear for different values of the magnetic field and their periods can be measured precisely.

(b) The oscillations appear in the same range of magnetic field but with different amplitudes; then they can be easily distinguished.

(c) Oscillations related to two almost equal periods appear in the same range of magnetic field and have similar amplitudes; the periods cannot be separated or at best, they are known with a large uncertainty.

B. Geometric Resonance

1. $\vec{q}$ *Along a Axis*

Geometric resonance was investigated in sample a1 at 158 and 303 MHz. At these frequencies geometric-resonance oscillations appear for magnetic fields smaller than 250 Oe. Such fields could be created by the Helmholtz coils and their value was known with an accuracy better than 1 Oe.

Figure 4 shows a typical recording of the oscillations in the bc plane as a function of the magnetic field at 303 MHz. Three types of oscillations can be observed.

(i) Type-A1 oscillations appear for all angular directions and for values of H in the range 50–200 Oe. The corresponding periods $\Delta(1/H)$ vary from 0.2×10^{-3} to 0.6×10^{-3} Oe^{-1}. One can observe 15–30 oscillations.

(ii) Type-A2 oscillations occur when the angle

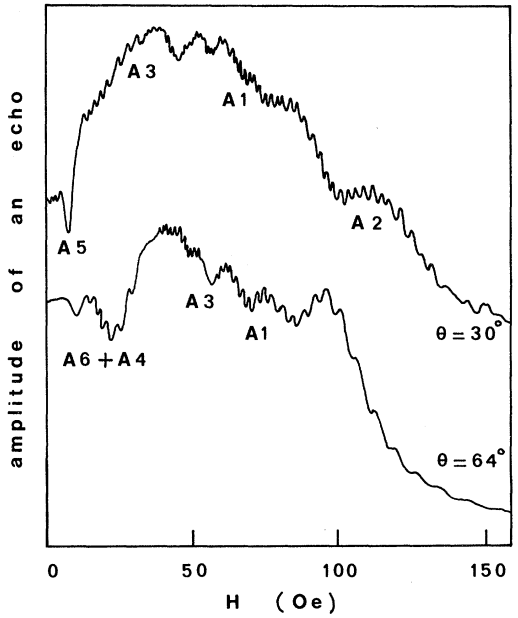

FIG. 4. Relative amplitude of an echo as a function of the applied magnetic field for a propagation along the a axis. θ is the angle between the direction of the magnetic field and the b axis. $f = 303$ MHz, $T = 1.25$ °K.

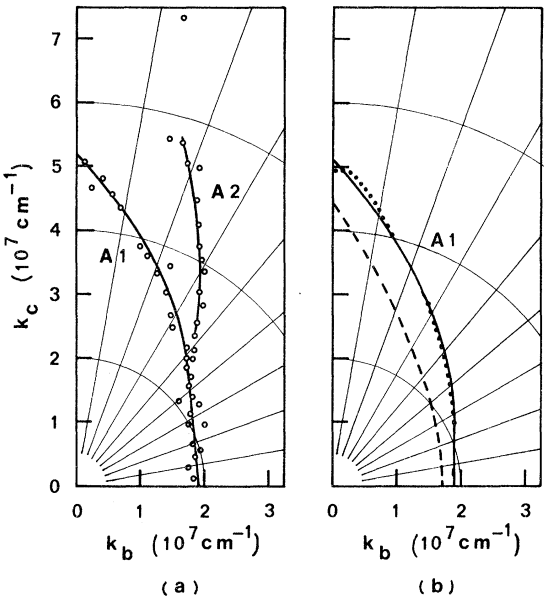

FIG. 5. Extremal dimensions of the Fermi surface in the $k_b k_c$ plane. (a) ○: Experimental points corresponding to A1 and A2 oscillations. (b) Comparison of line A1 to the extremal dimensions of the seventh-electron-band piece located at L. Solid line: line A1; dotted line: pseudopotential model; dashed line: APW model.

θ between the magnetic field and the b axis is contained between 10° and 45°, and when the magnetic field exceeds 120 Oe, i.e., the value for which the A1 oscillations start to vanish. This superposition of A1 and A2 reduces slightly the accuracy of A1 periods from 3% to 5%, since only 15–20 oscillations are seen in this case. The periods associated with the A2 oscillations are very close to those of A1, but the difference between the two is larger than the experimental uncertainty. Periods of A2 are known to within 5%.

(iii) Type-A3 oscillations are observed for all directions except those which are close to the c axis (up to 20° at 158 MHz and 8° at 303 MHz). The associated periods decrease from 0.45×10^{-2} to 0.15×10^{-2} Oe^{-1} when the direction of the magnetic field is rotated from the b axis towards the c axis. They are by an order of magnitude larger than A1 and A2 periods. Each period was determined using 8–10 oscillations and the corresponding accuracy on k_{ext} is better than 5%.

The results obtained for two different ultrasonic frequencies are in good agreement and the symmetries are clearly displayed. The corresponding extremal dimensions of the Fermi surface in the $k_b k_c$ plane are given in Figs. 5(a) and 6(a).

Let us now compare the experimental data with the results predicted by the APW and pseudopotential models. We ignore the nearly free-electron model with its prediction of a pseudo-hexagonal-symmetry in the $k_b k_c$ plane, which has never been observed experimentally. We will label the different sections of the Fermi surface in the same manner as the oscillations, that is A1, A2, and A3; for the principal symmetry directions in the central Brillouin zone we adopt the notation defined in Fig. 4 of Ref. 2.

Line A1 is compared in Fig. 5(b) to the extremal dimensions of the seventh-electron-band piece located at L. Our results are in very good agreement with the pseudopotential model. The corresponding values of k_{ext} in the APW model are systematically smaller, approximately by 10%. The same orbit has already been observed using the rf-size-effect (RFSE) technique.[17,18]

Type-C oscillations of Ref. 7 coincide exactly with line A2. Three points only were observed by Bezuglyi *et al.*[7] at 32°, 34°, and 36° from k_c. They were interpreted by Wood[3] as the section of the sixth-hole band by the plane $k_x = \pi/a$. However, our band A2 can be seen up to 17°, where the agreement is very unsatisfactory.

On Fig. 6(b) the experimental points A3 are compared to the cross section of the sixth-band piece located at T (which is a small flat ellipsoid according to the pseudopotential model) with the plane $k_a = 0$. We have also shown in this figure the intersection of the "monster leg" with the plane $k_a = 0$, as calculated from the APW model. This surface is an ellipse, but its extremal dimension

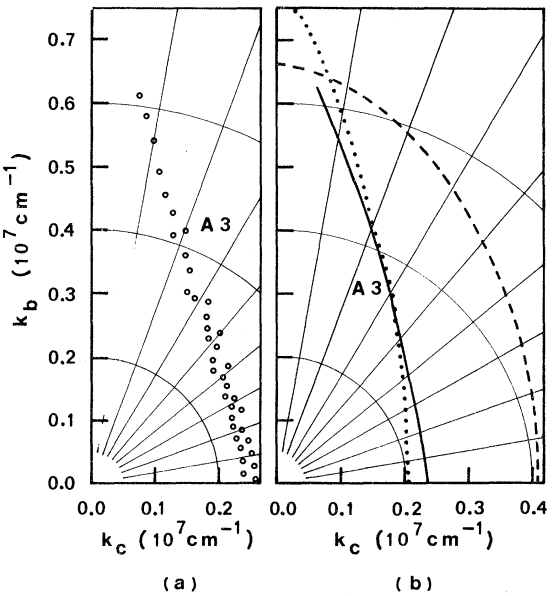

FIG. 6. (a) Extremal dimensions corresponding to A3 oscillations. (b) Comparison of line A3 to the cross section of the sixth-band piece located on T by the plane $k_a = 0$. Solid line: line A3; dotted line: pseudopotential model; dashed line: APW model.

TABLE III. Comparison of the extremal dimensions in the k_b and k_c directions of the sixth-band piece located on T, obtained from calculation and from different experimental techniques. Units: 10^7 cm^{-1}.

θ/k_c \ Method	Pseudo-potential	APW	RFSE (Ref. 18)	Geometric resonance (Ref. 7)	This work
0°	0.208	0.40	0.22	0.22	0.25
90°	0.775	0.66	0.72	0.41	0.725

along k_c is two-times larger than the corresponding experimental value (0.40×10^7 cm^{-1} instead of 0.23×10^7 cm^{-1}). In Table III, the extremal dimensions along the k_c and k_b axes obtained from different experimental techniques and from calculations are compared. One can see that our results are in good agreement with Reed's calculation.

2. $\vec{q}$ *Along b Axis*

Two samples were studied: b1 at 158 MHz and b2 at 72.5 MHz. Their parameters are given in Table I. The magnetic field was swept from 0 to 150 Oe.

Observe that the frequencies used in this case are smaller than in the former one. This was caused by the very strong attenuation α of the longitudinal ultrasonic waves along the b axis of gallium; for an ultrasonic frequency equal to 50 MHz, $\alpha = 25$ dB/cm at 1.2 °K. Since in our experiments $ql \gg 1$, α was proportional to the frequency, and for frequencies higher than 158 MHz the amplitude of the first echo was too small to allow any measurements. It was not possible to reduce the sample length sufficiently without introducing a limitation on the mean free path of the electrons. The striking feature of the results concerning propagation along the b axis is the very steep angular dependence of the oscillations, as shown in Fig. 7 for 72.5 MHz. Here θ is defined as the angle between the direction of the magnetic field and the c axis.

Three types of oscillations can be observed.

(a) When θ ranges from 10° to 50°, type-B1 oscillations are dominant. Their period, measured at 72.5 MHz, decreases from 2.2×10^{-3} to 0.5×10^{-3} Oe^{-1}. For θ smaller than 35°, only eight oscillations appear for magnetic fields varying between 25 and 40 Oe. When the magnetic field is rotated from 35° to 50° away from the c axis, the number of oscillations increases up to 40 or 50. These oscillations can be seen up to 150 Oe. In this case the precision with which k_{ext} can be determined is only limited by the uncertainty as to the values of the magnetic field, the ultrasonic frequency, and the sound velocity, and is smaller than 2%. For values of θ between 50° and 53°, B1 oscillations completely disappear. All the experiments performed on two different samples and at different ultrasonic frequencies confirm these results.

(b) Subdominant oscillations, called B2, appear for values of θ varying from 31° to 55° in the range 60–130 Oe, and the corresponding periods decrease from 1.60×10^{-3} to 1.07×10^{-3} Oe^{-1} at 72.5 MHz. Each period was determined using eight or nine oscillations, and the corresponding uncertainty of k_{ext} is 5%.

(c) Type-B3 oscillations were observed at 72.5 MHz, with θ contained between 0° and 60°, and magnetic fields in the range 15–40 Oe. The associated periods are of the order of 1.5×10^{-2} to 0.94×10^{-2} Oe^{-1}. Since they were calculated using four oscillations they are only known to within 10%.

The extremal dimensions associated with type-B1 and -B2 oscillations are shown in Fig. 8. The experimental curve B1 is compared to the orbit i defined by Reed.[4] This orbit is the intersection of the sixth-band surface with the plane $k_b = 0$. Although the experimental curve is interrupted at 10° off the k_a axis, which might be due to the reentrant shape of this orbit, the agreement with the theoretical shape of the sixth-band surface is very good.

We did not find any theoretical data fitting curve B2. However, a similar branch has already been observed experimentally by RFSE[17] and is shown in Fig. 8 of Ref. 17. These two experimental curves have the same shapes, but the extremal di-

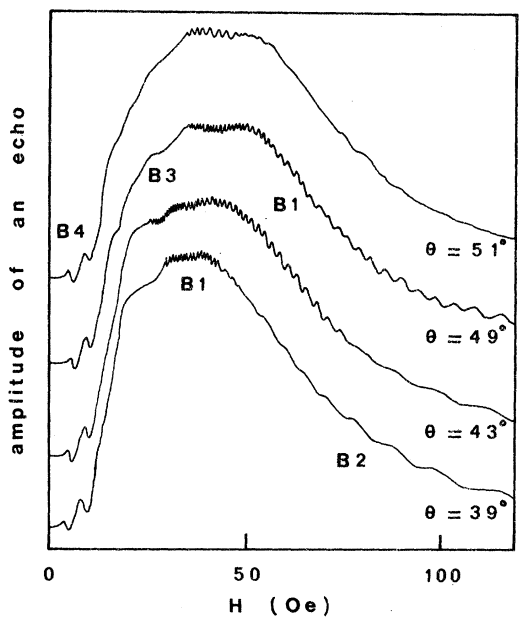

FIG. 7. Angular dependence of the oscillations observed in the ac plane, in sample b2. $f = 72.5$ MHz; θ is the angle between the direction of the magnetic field and the c axis.

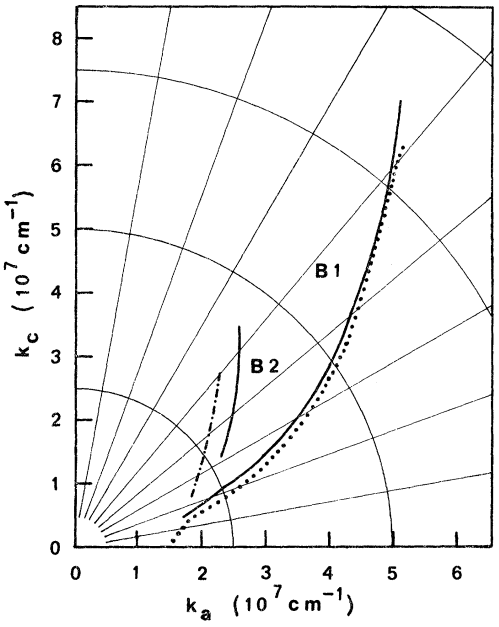

FIG. 8. Extremal dimensions of the Fermi surface corresponding to B1 and B2 oscillations. Solid line: mean experimental curves; dotted line: orbit i of the sixth-hole band of the pseudopotential model; dot-dashed line: branch observed by RFSE (Ref. 17).

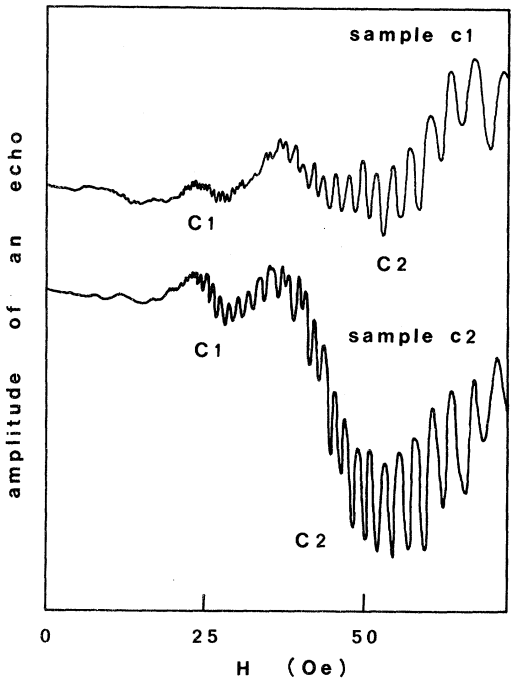

FIG. 10. Influence of the purity on ql and $\omega\tau$. $f=158$ MHz, θ/axis $a=70°$. In sample c2, the geometric-resonance oscillations C1 and the cyclotron-resonance oscillations are larger than in c1, because the conditions $ql \gg 1$ and $\omega\tau \gg 1$ are better satisfied.

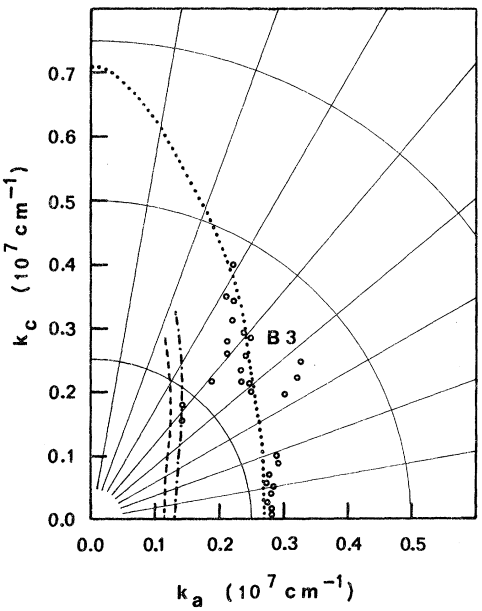

FIG. 9. Comparison of the extremal dimensions in the $k_a k_c$ plane associated to B3 oscillations, with the pseudopotential model. ○: experimental points; dotted line: intersection of the fifth-hole-band piece centered at X by the plane $k_b=0$; dot-dashed line: intersection of the seventh-electron-band piece located at U by the plane $k_b=0$; dashed line: geometric-resonance data from Ref. 8.

mensions we found are 15% larger.

In Fig. 9 the extremal dimensions associated with the B3 oscillations are compared to the intersection of the fifth-band surface centered at X with the plane $k_b=0$. We only consider the surface given by Reed's calculation, since the dimension along the k_a axis of the corresponding piece in the APW model is by an order of magnitude larger than the experimental one. The fit with the pseudopotential model is very good in the neighborhood of the k_a axis, where the extremal dimension is equal to 0.28×10^7 cm^{-1}.

The curve obtained by Bezuglyi *et al.*[8] by the same method is also shown in Fig. 9. Reed[4] suggested that this branch might be identified with the section of the seventh band centered on U by the plane $k_b=0$. In two directions, at angles 47° and 52° from k_a, we found extremal dimensions which coincide exactly with this theoretical curve. In these directions, however, the carriers which mainly contribute to the oscillations seem to be different from those which gave our branch B3.

3. $\vec{q}$ *Along c Axis*

Geometric resonance was investigated in the ab plane, at 158 and 303 MHz, in samples c1 and c2. The two samples have different purities: c1 was grown from gallium of 99.999% initial purity, and

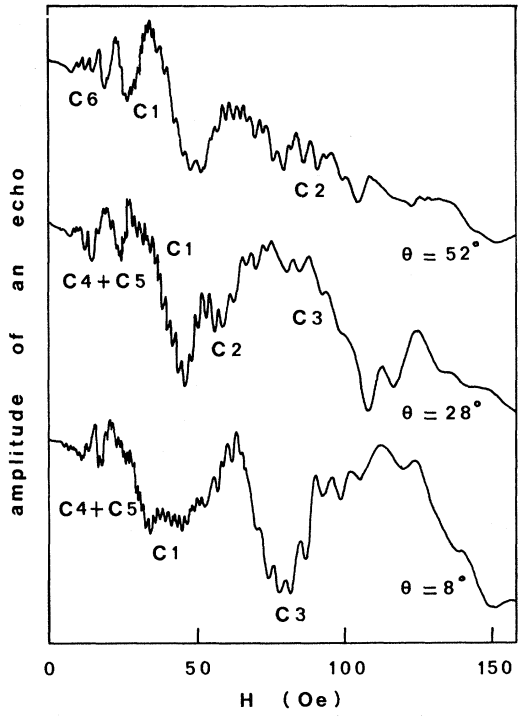

FIG. 11. Angular dependence of the oscillations observed in the *ab* plane in sample c2. $f=303$ MHz; θ is the angle between the direction of the magnetic field and the *a* axis.

*c*2 from 99.999 99% initial purity. The magnetic field was swept from 0 to 200 Oe; θ is defined here as the angle between the magnetic field and the *a* axis.

The influence of sample purity on the parameter ql is shown in Fig. 10. In both cases two types of oscillations, C1 and C2, appear and the condition $ql \gg 1$ is well satisfied. Nevertheless, the periods of small-amplitude oscillations such as type C1 can be measured with greater accuracy in sample c1 than in sample c2.

In Fig. 11 typical oscillations observed in the *ab* plane are shown.

Type-C1 oscillations appear for all angular directions. If θ is smaller than 15°, ten oscillations can be observed in the range 30–45 Oe, and for larger values of θ about 15 oscillations can be seen up to 60 Oe. The corresponding periods, which vary from 1.5×10^{-3} to 0.7×10^{-3} Oe^{-1} at 303 MHz, are known to within 5%.

Type-C2 oscillations can also be observed in all directions of the *ab* plane; their periods are shorter than those of type C1. About 15 oscillations can be counted in the range 60–200 Oe.

A third group of oscillations, C3, is present when θ varies from 0° to 30°. Near the *a* axis, for increasing values of the magnetic field, these oscillations appear just after C1; for θ between 20° and 30°, type-C3 oscillations follow after C1 and and C2.

The extremal dimensions associated with the periods measured on samples c1 and c2 at 158 and 303 MHz are shown in Fig. 12. The very good agreement between the data obtained in various experiments at different frequencies shows the accuracy of the transformation of the measurement of the ultrasonic attenuation into extremal dimensions of the Fermi surface. Some isolated points can be seen inside the so-called "butterfly wing"; the corresponding oscillations appear in the same magnetic range as C3's and their origin will be discussed together with branch C3.

In Fig. 13 we compare our curves C1 and C2 to the intersections of the seventh and eighth electron bands with the plane $k_c = 2\pi/c$. The general shape is similar in the two theoretical models, but the experimental data fitted the pseudopotential model better, especially near the k_a axis. The surfaces under consideration are already well known and our results are in good agreement with those previously reported.[9,17,18]

The values ascribed to type-C3 oscillations and to the earlier mentioned isolated points are shown in Fig. 14. An uncertainty remains with regard to the identification of the pieces of the Fermi surface corresponding to these points. Different schemes can be proposed.

(i) For all directions within 40° from the k_b axis our results coincide well enough with curve

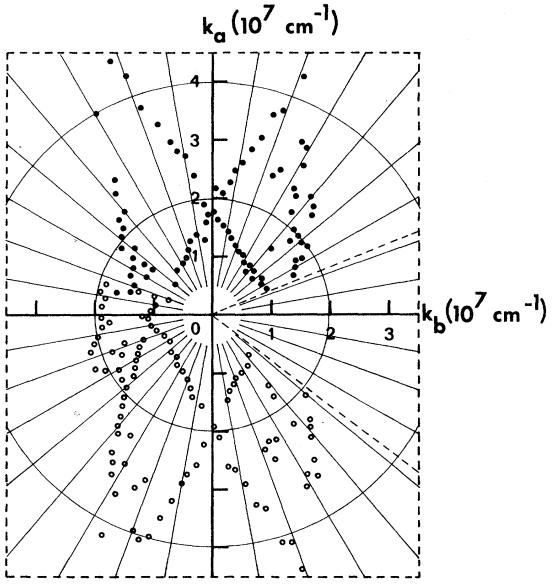

FIG. 12. Extremal dimensions of the Fermi surface measured in the $k_a k_b$ plane. ○: $f=303$ MHz, sample c2; ●: $f=158$ MHz, sample c1. The angular range which was investigated extends from 23° to 343°.

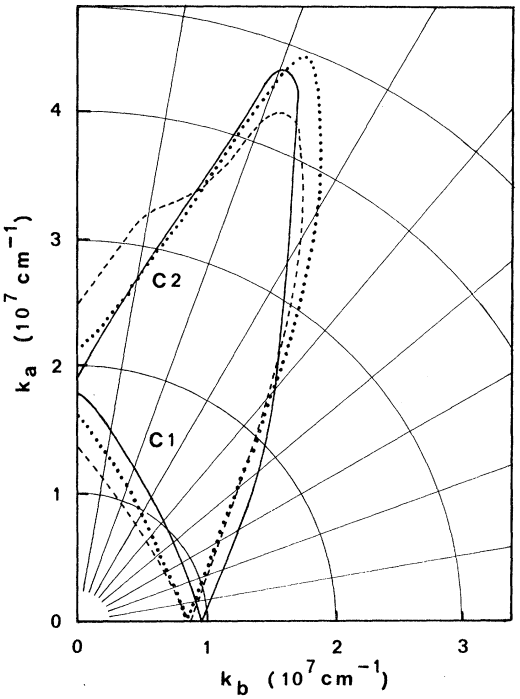

FIG. 13. Comparison of the curves C1 and C2 to the intersections of the seventh and eighth electron bands with the plane $k_c = 2\pi/c$. Solid line: experimental curves; dotted line: pseudopotential model; dashed line: APW model.

11 observed by RFSE.[17] Reed[4] showed that this curve may be associated with an extremal orbit of the sixth-hole band, labeled orbit 11 on Fig. 5 of Ref. 4. If we consider that the points which appear in the range 50°–70° from the k_b axis correspond to the same extremal orbit, then our branch is slightly longer than the theoretical one in the k_a direction.

(ii) In the directions within 40° of the k_b axis, the experimental points are associated with an extremal orbit. Between 40° and 50° the carriers which have such an orbit have a decreasing contribution to the oscillations. To the contrary, electrons of another extremal orbit become more and more important and give the dominant oscillations for angles larger than 50°.

(iii) The C5 branch of Ref. 18, observed by RFSE, is shown in Fig. 14. This branch was identified as the intersection of the fifth-hole band centered at X with the plane $k_c = 0$ in the APW model. Some of our points, for θ varying from 50° to 65°, might be associated with this branch. However, this hypothesis would disagree with the interpretation we gave for branch B3. This branch was associated with an orbit of the fifth-band surface centered at X, in good agreement with the pseudopotential model. Since the dimensions of this piece of Fermi surface in the APW model are one order of magnitude larger than in the pseudopotential model, it is not possible to interpret one cross section in the first model and another in the second.

Among these possibilities, the most likely seems to be that for angles ranging from 0° to 40°, the observed oscillations should be associated to orbit 11, and that for $\theta > 40°$ carriers of an unidentified orbit have the dominant contribution to the oscillations.

4. *Summary of Geometric-Resonance Data*

In Table IV we have listed the observed branches together with the extremal orbits used to interpret them as given by the theoretical models. All the branches but A2 and B2 can be identified in the pseudopotential model. No definite explanation could be given for A2 and for B2, which have too small angular extent to allow a precise comparison. The main difference between the two theoretical models is found in the shapes of the fifth- and sixth-hole bands. Our experimental results show that the pseudopotential method gives the best fit for these pieces of the Fermi surface of gallium.

C. Acoustic Cyclotron Resonance

1. $\vec{q}$ *Along a Axis*

The condition $\omega\tau \gg 1$ required to observe ACR implies that the ultrasonic frequency must be as

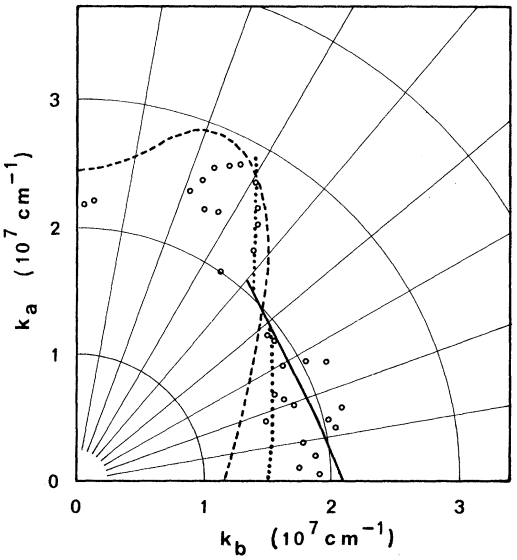

FIG. 14. ○: extremal dimensions associated with C3 oscillations. Solid line: orbit 11 obtained by RFSE (Ref. 17) and calculation; dotted line: branch C5 observed by RFSE (Ref. 18); dashed line: intersection of the fifth-hole band centered at X by the plane $k_c = 0$, from the APW model.

TABLE IV. Identification of the experimental curves using the APW and pseudopotential model. Seventh electron band at L point is abbreviated $7e$ at L, etc.

This work	Pseudopotential model	APW model
A1	$7e$ at L	$7e$ at L
A2		
A3	$6h$ at T	
B1	$6h$ (orbit i)	
B2		
B3	$5h$ at X	
C1	$8e$ at L	$8e$ at L
C2	$7e$ at L	$7e$ at L
C3	$6h$ (orbit 11)	

large as possible. At 303 MHz, ACR oscillations can be observed in sample a1, whereas at 158 MHz only the strongest oscillations can be seen, but they do not allow a quantitative study. It could be concluded that the condition $\omega\tau \gg 1$ is not satisfied at 150 MHz, while for an ultrasonic frequency equal to 300 MHz the line shape of the oscillations suggests that $\omega\tau \simeq 10$. With this value, the collision time at 1.25 °K, in this 99.999 99%-purity gallium sample, is of the order of 5×10^{-8} sec.

The angular variation of ACR oscillations in the bc plane is shown in Fig. 4. Three types of oscillations can be distinguished.

(a) When the angle θ between the direction of the magnetic field and the b axis is in the range 0°–40°, two large oscillations, called A5, appear for values of the magnetic field smaller than 10 Oe. The periods $\Delta(1/H)$ vary from 9.5×10^{-2} to 12.1×10^{-2} Oe^{-1}, and the corresponding ratios m^*/m_0 can be calculated using (4). The ratios vary from $0.08m_0$ to $0.1m_0$. We must point out that these values are subject to a large uncertainty for two reasons. First, the period is determined by only two oscillations. Second, the uncertainty on the value of the magnetic field is of the order of 1 Oe. As the oscillations appear for very low values of H, the corresponding error on $\Delta(1/H)$ is quite large. In the angular range 0°–20°, we estimate that the uncertainty on the effective masses belonging to branch A5 is 20%. In the range 20°–40° the uncertainty is even larger, because another set of oscillations of small amplitude is superimposed on the A5 oscillations. For this reason we do not give the relevant values of the masses.

(b) When θ is varying from 50° to 90°, two types of oscillations can be observed. Only two A6-type oscillations appear, at magnetic fields close to 19 and 10 Oe. The corresponding periods vary with θ from 5.4×10^{-2} to 6.3×10^{-2} Oe^{-1} and the effective masses from $0.18m_0$ to $0.14m_0$. The line $1/H_n = f(n)$ passes, within the experimental error, through the origin. This indicates that the oscillation which occurs at 19 Oe corresponds to the fundamental resonance. Moreover, the symmetry with respect to the c axis is clearly observed. This reduces to 10% the uncertainty on the effective masses belonging to branch A6.

Another group of oscillations, labeled A4, corresponds to small periods and is superimposed on the fundamental A6-type oscillation. These oscillations appear for fields between 16 and 40 Oe and their period increases from 0.6×10^{-2} to 0.75×10^{-2} Oe^{-1}. Up to seven oscillations can be observed, and the corresponding effective masses, ranging from $1.65m_0$ to $1.27m_0$, are known to within 5%.

A map of the effective masses in the bc plane is shown in Fig. 15(a). These data can be compared to those obtained using the Azbel'–Kaner-cyclotron-resonance (AKCR) method.[19,20] In the following, we will only consider the data published by Moore[19] which are the most detailed ones.

Our curve A4 can be compared to branch λ of Ref. 19. The fit between these two curves is good for values of θ near 50° but a discrepancy appears near the c axis, where the values of m^* on branch A4 become larger than those of branch λ. Moreover, branch λ is interrupted at 10° from the c axis, whereas we can see the A4 oscillations even along the c direction.

Branch A5 is identified as a part of branch c of Ref. 19. In the angular range where the periods A5 can be measured, the effective masses are of the order of $0.08m_0$, while those of curve c are close to $0.06m_0$. This difference is of the same order as our experimental error.

The correspondence between branch A6 and branch M' of Ref. 19 is almost perfect. The value of the effective mass along the c axis is $0.14m_0$ and at 30° from this axis it is equal to $0.17m_0$. It should be pointed out, however, that branch M' has been observed in a larger angular range than A6 (50° instead of 30°).

2. $\vec{q}$ *Along b Axis*

We already mentioned that longitudinal waves are strongly attenuated when propagated along the b axis of high-purity single crystals of gallium and that the highest frequency we could reach was equal to 158 MHz. At this frequency the condition $\omega\tau > 1$ is just satisfied, so that very reduced data could be obtained in the ac plane.

For all directions of the magnetic field in this plane, two or three oscillations have been observed. Several experimental points have been eliminated because of a lack of symmetry.

In the range 32°–55° from the c axis, type-B4 oscillations have been observed, as shown in Fig. 7. These oscillations appear for small values of the magnetic field, between 5 and 10 Oe, and con-

sequently the uncertainty on the associated effective masses is about 15%. The values of the effective masses, which increase from $0.35m_0$ to $0.45m_0$, are listed in Fig. 15(b). No correspondence could be established with the results of Moore.

3. $\vec{q}$ *Along c Axis*

ACR has been investigated at 300 MHz using samples c1 and c2. In all angular directions at least two periods could be observed. On the recording shown in Fig. 11, ACR oscillations are the large oscillations which appear for values of the magnetic field smaller than 80 Oe.

When θ, the angle between the direction of the magnetic field and the a axis, varies from 0° to 40°, three dominant oscillations appear in the range 15–70 Oe. The corresponding periods decrease from 2.9×10^{-2} to 1.5×10^{-2} Oe^{-1} for increasing values of θ, and the associated effective masses are labeled C4 in Fig. 15(c). In some directions in the same angular range another set of six oscillations, C5, of amplitude and period smaller than C4 oscillations, has been observed. The superposition of these two types of oscillations increases the uncertainty on the values of the C4 and C5 effective masses up to 20%. The effective masses associated with C5 oscillations form a group of experimental points labeled C5 in Fig. 15(c); their values are in the range $0.7m_0$–$0.8m_0$.

When θ is varied from 40° to 75°, a third type of oscillations, called C6, appears for magnetic fields in the range 7–70 Oe. A typical example of C6 oscillations is given in Fig. 11 for $\theta = 52°$. The corresponding periods, which have been determined using six or seven oscillations, decrease with increasing values of θ; the associated effective masses can be seen on branch C6 of Fig. 15(c). The uncertainty on the effective masses belonging to branch C6 is 5%. It is possible to notice the very small dispersion of the experimental points around branch C6, as compared to that of branches C4 and C5. Let us point out that the resonant fields, which are known with a good accuracy because the only other period superim-

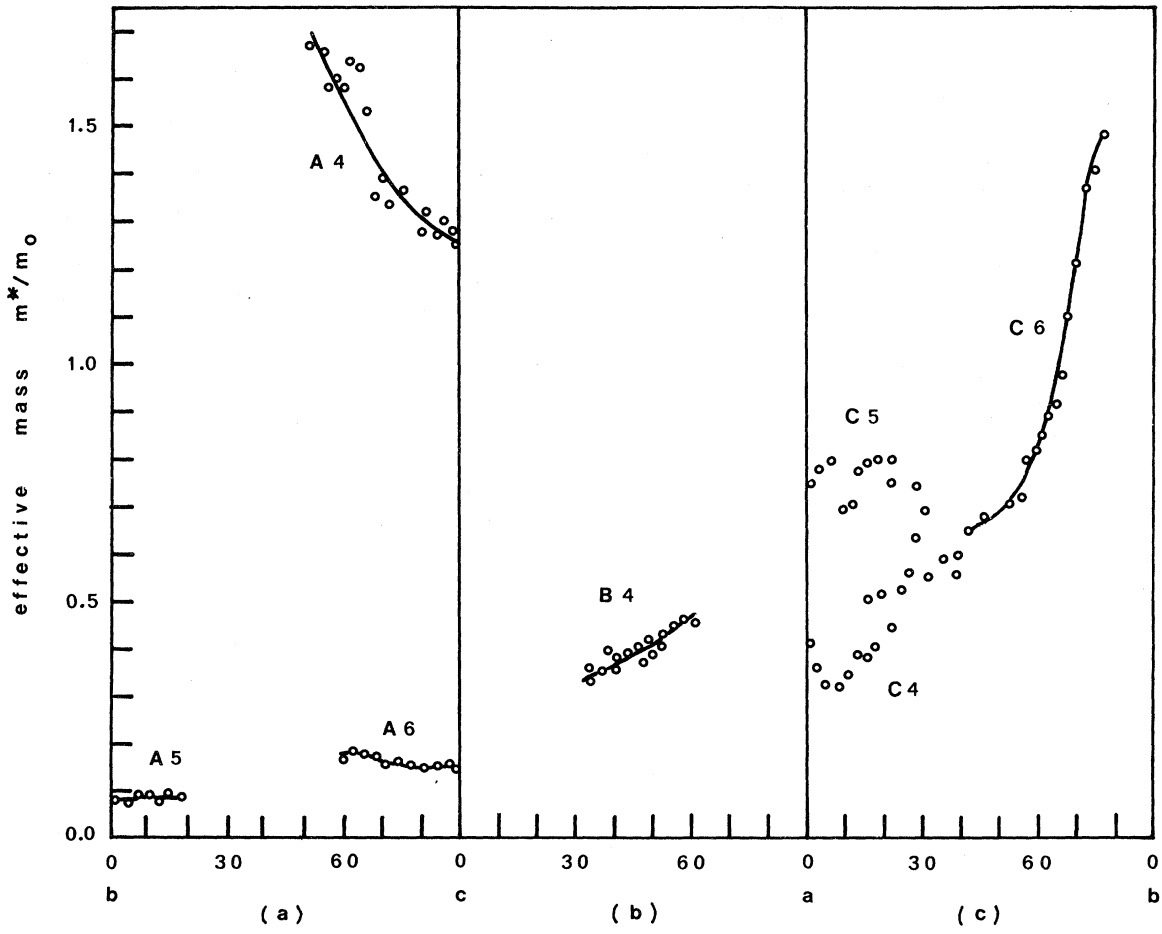

FIG. 15. Reduced effective masses obtained by ACR (a) in the *bc* plane, (b) in the *ca* plane, (c) in the *ab* plane.

posed on C6 appears for very low fields (10–20 Oe), exhibit a characteristic phase shift, as was already reported.[12]

Let us compare our results in the *ab* plane to both those obtained by Moore[19] using AKCR and those of Ref. 10 using ACR.

Branch C4 can be compared to the AKCR branch M and to the ACR branch I. The agreement is limited to values of θ smaller than 10° and is very good on the *a* axis ($\theta = 0°$), the effective mass being equal to $0.35 m_0$. For larger values of θ, the effective masses belonging to branch C4 increase more than those of branch M and branch I, so that they might correspond to different orbits.

The points of group II observed in Ref. 10 are contained in group C5. This confirms the existence of a set of effective masses which have not been observed by AKCR. Branch III of Ref. 10 is clearly a part of our branch C6. There is no equivalent branch in the data obtained by AKCR.

IV. CONCLUSION

Geometric-resonance experiments have been carried out in the three principal crystallographic planes of single crystals of gallium. The extremal dimensions of the Fermi surface which have been determined using this technique are in good agreement with the already existing data. Some new branches have been observed, particularly branch B1, which has a large angular extent.

Our results are in good agreement with the pseudopotential model developed by Reed. It seems that the shape of the fifth- and sixth-hole bands predicted by this model is quite satisfactory and the fit with the other bands, which were better known, is very good.

Using the ACR technique, a map of effective masses in the *ab*, *bc*, and *ca* planes has been drawn. Some branches have been observed which do not appear in the AKCR data, but reciprocally many AKCR curves have no equivalent in our data. The uncertainty of our experimental results remains too large for ACR to be competitive with the AKCR method. In order to reduce this uncertainty it would be necessary to increase the frequency of the ultrasonic wave—a rather difficult step because of the associated increase in the wave attenuation.

---

[1]A complete bibliography of the experimental studies prior to 1969 can be found in Ref. 2 of W. A. Reed, Phys. Rev. 188, 1184 (1969). Another paper was published later by J. R. Cook and W. R. Datars [Phys. Rev. B 1, 1415 (1970)].

[2]J. C. Slater, G. F. Koster, and J. H. Wood, Phys. Rev. 126, 1307 (1962).

[3]J. H. Wood, Phys. Rev. 146, 432 (1966).

[4]W. A. Reed, Phys. Rev. 188, 1184 (1969).

[5]B. W. Roberts, Phys. Rev. Letters 6, 453 (1961).

[6]P. Biquard, J. N. Aubrun, A. Bourret, and D. Launois, J. Phys. Radium 23, 954 (1962).

[7]P. A. Bezuglyi, A. A. Galkin, and S. E. Zhevago, Zh. Eksperim. i Teor. Fiz. 47, 825 (1964) [Sov. Phys. JETP 20, 552 (1965)].

[8]P. A. Bezuglyi, A. A. Galkin, and S. E. Zhevago, Fiz. Tverd. Tela 7, 480 (1965) [Sov. Phys. Solid State 7, 383 (1965)].

[9]J. Lewiner, Compt. Rend. 265B, 774 (1967).

[10]J. Lewiner, Phys. Rev. Letters 19, 1037 (1967).

[11]J. A. Munarin, Phys. Rev. 172, 737 (1968).

[12]C. Alquie and J. Lewiner, Phys. Rev. B 5, 2749 (1972).

[13]M. H. Cohen, M. J. Harrison, and W. A. Harrison, Phys. Rev. 117, 937 (1960).

[14]W. C. Overton, Jr. and J. Gaffney, Phys. Rev. 98, 969 (1955).

[15]H. J. McSkimin, J. Acoust. Soc. Am. 33, 12 (1961).

[16]K. R. Lyall and J. F. Cochran, Can. J. Phys. 49, 1075 (1971).

[17]A. Fukumoto and M. W. P. Strandberg, Phys. Rev. 155, 685 (1967).

[18]P. H. Haberland, J. F. Cochran, and C. A. Shiffman, Phys. Rev. 184, 655 (1969).

[19]T. W. Moore, Phys. Rev. 165, 864 (1968).

[20]M. Surma, Acta Phys. Polon. 32, 677 (1967); 34, 387 (1968).